Coherent transients mimicked by two-photon coherent control of a three-level system

Jongseok Lim, Han-gyeol Lee, Jae-uk Kim, Sangkyung Lee, and Jaewook Ahn*
Department of Physics, KAIST, Daejeon 305-701, Korea
(Received 24 December 2010; revised manuscript received 21 March 2011; published 26 May 2011)

We show theoretically and experimentally that two-photon coherent control in a V-shape three-level system projects a one-photon coherent transient in a simple two-level system. The second- and third-order spectral phase terms of a shaped laser pulse play the roles of time and quadratic spectral phase, respectively, in conventional coherent transients. In a three-pulse coherent control experiment of atomic rubidium, the phase and amplitude of controlled transition probability is retrieved from a two-dimensional Fourier-transform spectral peak. It is hoped that this control scheme may harness coherent control capability on multidimensional Fourier-transform spectroscopy.

DOI: 10.1103/PhysRevA.83.053429 PACS number(s): 32.80.Qk, 32.80.Wr, 42.50.Md, 42.65.Re

I. INTRODUCTION

Recent advances in ultrafast laser and optical pulse shaping techniques have brought the use of shaped pulses of optical frequency for the manipulation of quantum systems [1–4]. This field, known as quantum control, though being started as a theoretical exercise, has rapidly become an experimental reality in a vast variety of materials extending from atoms and molecules to condensed matter and biological materials [5–9].

One of the simplest ways to shape an optical pulse is to chirp or to make a quadratic spectral phase, i.e.,

$$\phi(\omega) = \frac{a_2}{2}(\omega - \omega_0)^2, \tag{1}$$

where a_2 is the linear chirp rate and ω_0 the laser center frequency. Chirped pulses have been used to control molecular vibrational excitation and fragmentation [10,11], coherent anti-Stokes Raman scattering microscopy [12], molecular alignments [13], and high harmonic generation [14], to list a few. Of particular relevance in the context of the present paper is the chirped pulse excitation of atoms in the weak-field interaction regime, also known as coherent transients (CTs) [15–17].

As a brief review of CTs, we consider one-photon transition in a two-level system of ground state $|1\rangle$ and excited state $|2\rangle$. For an optical short pulse of Gaussian pulse shape with chirp, the electric field $E(t)$ is given by

$$E(t) = \mathcal{E}_o \exp\left[-\frac{t^2}{\tau_c^2} - i(\omega_0 t + \alpha t^2)\right], \tag{2}$$

where $\tau_c = \tau_o\sqrt{1+a_2^2/\tau_o^4}$, $\alpha = 2a_2/(\tau_o^4 + 4a_2^2)$, and τ_o is the unchirped pulse duration. Then the excitation probability amplitude c_{21} at a finite time t is given in the weak-field regime as [17]

$$c_{21}(t) = \frac{i\mu_{21}\mathcal{E}_o}{\hbar}\int_{t_0}^{t} \exp\left(-\frac{t'^2}{\tau_c^2}\right) \times \exp\{-i[(\omega_0 - \omega_{21})t' + \alpha t'^2]\}dt', \tag{3}$$

where the time t and the linear chirp rate a_2 are the two control parameters for the quadratic and cubic phase terms, respectively, and the finite time integration with a quadratic temporal phase $\alpha t'^2$ leads to the transient excited-state population being of a Cornu spiral shape, well known from Fresnel diffraction patterns from a sharp edge [18]. For a short pulse which has broad spectral components, putting chirp on the pulse delays some of those components with respect to others in the time domain, and the instantaneous laser frequency shifts as a function of time. So, from the time when the resonant condition is met, further off-resonant excitation interferes with the resonant transition, either constructively or destructively. In the frequency domain representation, Eq. (3) is given by

$$c_{21}(t) = \frac{\mu_{21}}{\hbar}\left[i\pi\widetilde{E}(\omega_{21}) + \mathrm{P}\int_{-\infty}^{\infty}\frac{\widetilde{E}(\omega)\exp[i(\omega_{21}-\omega)t]}{\omega_{21}-\omega}d\omega\right], \tag{4}$$

where $\widetilde{E}(\omega) = E_o\exp[-(\omega-\omega_0)^2\tau_o^2/4 + i\phi(\omega)]$ and P is the Cauchy principal value [19]. So, the quantum interference between the resonant and nonresonant excitation contributions shows an oscillatory transient behavior for a given chirped pulse. CTs have demonstrated many novel phenomena, including the time-domain Fresnel lens [16], coherent transient enhancements [19], quantum-state holographic measurements [20], and coherent controls of multistate ladders [21].

In this paper we show that the conventional CT in a simple two-level system is mimicked by two-photon coherent control in a V-shape three-level system. Higher order chirps of a shaped laser pulse play the roles of time and linear chirp in CTs. For this, we consider two-photon control of a three-level system in V-type configuration [22]. We note that the controlled transitions in a two-level system or in a three-level ladder-type system are readily monitored by detecting the fluorescence decay from the target excited state [23–26]. On the other hand, the two-photon interexcited state transition in a V-type quantum system is not straightforward to measure and thus has been difficult to control. It is because the state population of the target excited state is coherently mixed with the dominant one-photon transition population from the ground state. We report in this paper that this difficulty is overcome with the combined use of two-dimensional Fourier-transform spectroscopy (2D-FTOS) [27–29] and a coherent control technique.

*jwahn@kaist.ac.kr

The paper is organized as follows: In Sec. II, after describing the model, we show that with a chirped pulse of up to cubic phase, i.e.,

$$\phi(\omega) = \frac{a_2}{2}(\omega - \omega_0)^2 + \frac{a_3}{6}(\omega - \omega_0)^3, \tag{5}$$

the given two-photon coherent control of a V-type system is reduced to the discussed CT in a two-level system, where now a_2 and a_3 play the roles of the time and linear chirp in a regular CT. Section III is devoted to the experimental description where the three-pulse coherent control scheme devised in the Appendix is used to measure the two-photon interexcited state transition in a 2D-FTOS setting. In Sec. IV we present the experimental results before concluding in Sec. V.

II. THEORETICAL MODEL

The model atomic system is in V-type configuration, composed of ground state $|g\rangle$ and two excited states $|a\rangle$ and $|b\rangle$, with respective energies $\hbar\omega_g$, $\hbar\omega_a$, and $\hbar\omega_b$. The excited states are dipole-coupled to the common ground state, with dipole moments μ_{ag} and μ_{bg}, and the transition between the excited states is forbidden (i.e., $\mu_{ab} = 0$). Then the Hamiltonian is given by

$$H(t) = H_0 + V(t), \tag{6}$$

where $H_0 = \sum_i \hbar\omega_i |i\rangle\langle i|$ and $V(t) = -\sum_{i,j} \mu_{ij} E(t) |i\rangle\langle j|$ for $i,j \in \{g,a,b\}$. With $T = \exp(-iH_0 t/\hbar)$, we transform to the interaction picture, obtaining the interaction Hamiltonian

$$H_I(t) = T^\dagger H(t) T + i\hbar \frac{dT^\dagger}{dt} T = \sum_{i,j} V_{ij}(t) e^{i\omega_{ij} t} |i\rangle\langle j|, \tag{7}$$

where $V_{ij}(t) = \langle i|V(t)|j\rangle$ and $\omega_{ij} = \omega_i - \omega_j$. Then the transition probability amplitude from state $|i\rangle$ to state $|f\rangle$, defined by

$$c_{fi}(t) = \langle f|U_I(t,t_0)|i\rangle, \tag{8}$$

where $U_I(t,t_0)$ is the evolution operator given by

$$U_I(t,t_0) = 1 - \frac{i}{\hbar}\int_{t_0}^{t} H_I(t') U_I(t',t_0) dt', \tag{9}$$

is obtained by the order of $V(t)$ as

$$c_{fi}^{(0)}(t) = \delta_{fi}, \tag{10}$$

$$c_{fi}^{(1)}(t) = -\frac{i}{\hbar}\int_{t_0}^{t} dt' V_{fi}(t') \exp(i\omega_{fi} t'), \tag{11}$$

$$c_{fi}^{(2)}(t) = \left(-\frac{i}{\hbar}\right)^2 \Sigma_j \int_{t_0}^{t} dt' \int_{t_0}^{t'} dt'' \times V_{fj}(t') V_{ji}(t'') \exp(i\omega_{fj} t' + i\omega_{ji} t''). \tag{12}$$

For an electric field shaped in the frequency domain as

$$\widetilde{E}(\omega) = A(\omega) e^{i\phi(\omega)}, \tag{13}$$

where $A(\omega)$ is spectral amplitude and $\phi(\omega)$ is spectral phase, the time domain pulse profile is given by

$$E(t) = \frac{1}{\sqrt{2\pi}}\int_{-\infty}^{\infty} \widetilde{E}(\omega) e^{-i\omega t} d\omega, \tag{14}$$

where the imaginary part of $E(t)$ is maintained zero all the time by defining $\widetilde{E}(-\omega) = \widetilde{E}^*(\omega)$ for $\omega < 0$. Then $V_{ij}(t) = -\mu_{ij} E(t)$, and the first-order (one-photon) transition probability amplitude is simply the corresponding spectral amplitude given by

$$c_{fi}^{(1)} = i\frac{\mu_{fi}}{\hbar}\sqrt{2\pi}\,\widetilde{E}(\omega_{fi}), \tag{15}$$

where we consider the integral limit $[t_0,t] \to [-\infty,\infty]$ by assuming the pulse duration is considerably shorter than all lifetimes involved.

Now we consider the two-photon transition probability amplitude between the excited states $|a\rangle$ and $|b\rangle$. From Eq. (12) we obtain the second-order interexcited state transition probability amplitude as

$$c_{ba}^{(2)} = i\frac{\mu_{ga}\mu_{gb}}{\hbar^2}\left[i\pi \widetilde{E}^*(\omega_{ag})\widetilde{E}(\omega_{bg}) - \mathrm{P}\int \frac{\widetilde{E}^*(\omega)\widetilde{E}(\omega_{ba}+\omega)}{\omega_{ag}-\omega} d\omega\right], \tag{16}$$

which is similar to Ref. [15] of a ladder-type three-level system, except for minor details.

For a Gaussian pulse spectrally centered at ω_0, i.e., $A(\omega) = E_0 \exp[-(\omega-\omega_0)^2/\Delta\omega^2]$, with the spectral phase $\phi(\omega)$ given in Eq. (5), the transition probability amplitude Eq. (16) is simplified to the following form:

$$c_{ba}^{(2)} = i\frac{\widetilde{\mu}_{ba}}{\hbar^2}\left[i\pi\widetilde{\mathbb{E}}(\overline{\omega}) - \mathrm{P}\int_{-\infty}^{\infty}\frac{\widetilde{\mathbb{E}}(\omega)}{\overline{\omega}-\omega} d\omega\right], \tag{17}$$

where $\widetilde{\mu}_{ba} = \mu_{ga}\mu_{bg}\exp[-\omega_{ba}^2/2\Delta\omega^2 + ia_3\omega_{ba}^3/24]$, $\overline{\omega} = (\omega_{ag}+\omega_{bg})/2$, and

$$\widetilde{\mathbb{E}}(\omega) = E_o^2 \exp\left[-2\frac{(\omega-\omega_0)^2}{\Delta\omega^2} + i\omega_{ba}\frac{d\phi}{d\omega}\right]. \tag{18}$$

It is noted that Eq. (17) is of a functional form strikingly similar to Eq. (4), the one-photon transition in a two-level system, except for the sign between the resonant and nonresonant contributions. The difference between Eq. (4) and Eq. (17) is resolved by considering a de-excitation. For an electric field of Gaussian pulse shape with linear chirp (only), the one-photon transition probability amplitude from $|2\rangle$ to $|1\rangle$ is easily found as

$$c_{12}^{(1)}(t) = \frac{\mu_{21}}{\hbar} e^{-i(\omega_{21}-\omega_0)t}\left[i\pi E^*(\omega_{21}) e^{i(\omega_{21}-\omega_0)t} - \mathrm{P}\int_{-\infty}^{\infty}\frac{E^*(\omega)e^{i(\omega-\omega_0)t}}{\omega_{21}-\omega} d\omega\right]. \tag{19}$$

As evident from the same structure, the two-photon interexcited state transition in a V-type system projects one-photon transition (de-excitation) in a simple two-level system. The tantalizing part is that since $\widetilde{\mathbb{E}}(\omega)$ has a differentiated phase, linear chirp in the V-shape system corresponds to time in a two-level system, and minus quadratic chirp to linear chirp. So, the obtained solution in Eq. (17), which is the transition probability amplitude $c_{ba}^{(2)}$ for the two-photon interexcited state transition in a V-type system, has become formally a one-photon transition probability amplitude, more specifically,

a de-excitation process in a two-level system of energies 0 and $\overline{\omega}$, induced by the newly defined electric field $\widetilde{\mathbb{E}}(\omega)$.

Therefore if we consider the interaction of the V-shape system with a laser-shaped pulse of linear and quadratic chirps, then we can achieve duplicated results of coherent transients in a two-level system interacting with a linearly chirped pulse. With this information, we can derive the "transient" excitation probability amplitude, a similar form to Eq. (3), for the V-shape system. For this, the electric field $\mathbb{E}(t)$ is the inverse Fourier transformation of the complex conjugate of the electric field in frequency domain $\widetilde{\mathbb{E}}(\omega)$, having $\widetilde{t} = \omega_{ba} a_2$ $(t = 0)$ and $\widetilde{a}_2 = -\omega_{ba} a_3$. Then, the "CT-like" transition probability amplitude in a V-shape system is obtained as

$$c_{ba}^{(2)}(a_2,a_3) = -\frac{\widetilde{\mu}_{ba} E_o^2 e^{i\theta}}{\hbar^2} \frac{\Delta\omega}{\sqrt{\widetilde{\tau}_c/\widetilde{\tau}_0}} \int_{-\infty}^{\widetilde{t}} \exp\left(-\frac{t'^2}{\widetilde{\tau}_c^2}\right) \times \exp\{-i[(\omega_{ba}-\omega_0)t' - \widetilde{\alpha} t'^2]\} dt', \quad (20)$$

where $\theta = -\frac{1}{2}\tan^{-1} 2\widetilde{a}_2/\widetilde{\tau}_o^2 + (\overline{\omega}-\omega_0)\widetilde{t}$, $\widetilde{\tau}_o = 2\sqrt{2}/\Delta\omega$, $\widetilde{\tau}_c = \widetilde{\tau}_o\sqrt{1+\widetilde{a}_2^2/\widetilde{\tau}_o^4}$, and $\widetilde{\alpha} = 2\widetilde{a}_2/(\widetilde{\tau}_o^4 + 4\widetilde{a}_2^2)$.

III. EXPERIMENTAL DESCRIPTION

The two-photon control in the previous section can be verified by measuring the phase and amplitude of $c_{ba}^{(2)}(a_2,a_3)$. This is achieved by using the three-pulse coherent control scheme to be described in the Appendix. To summarize briefly, we need three optical pulses among which the second pulse (β) is the control pulse shaped to induce two-photon interexcited state transition from $|a\rangle$ to $|b\rangle$ [see Fig. 1(a)]. Prior to the second pulse, the atoms need to be excited to $|a\rangle$ by the first pulse (α). In addition, the third pulse (γ) induces the quantum interference which is used to measure $c_{ba}^{(2)}(a_2,a_3)$. After all three interactions, the excited state population $P_b(\tau_1,\tau_2)$ is measured as a function of two time intervals τ_1 and τ_2. Then from the 2D Fourier-transform spectrum of $P_b(\tau_1,\tau_2)$, that is, $S(\omega_1,\omega_2)$, the spectral peak located at $(\omega_1,\omega_2) = (\omega_{ag}-\omega_0, \omega_{bg}-\omega_0)$ reveals the controlled transition probability amplitude $c_{ba}^{(2)}(a_2,a_3)$.

For the experiment, we used the lowest three energy levels of atomic rubidium [see Fig. 1(b)]. The energy states $|a\rangle = |5P_{1/2}\rangle$ and $|b\rangle = |5P_{3/2}\rangle$ were resonantly excited from the common ground state $|g\rangle = |5S_{1/2}\rangle$, so these three energy states comprise an ideal V-shape coupled system. The experimental setup is shown in Fig. 1(c). The sequence of temporally and spectrally designed ultrafast pulses was produced from an acousto-optic programmable dispersive filter [30] assembled in a Ti : sapphire multipass laser amplifier operating at 1 kHz. The laser pulse duration was 35 fs, and the laser spectrum was centered at 800 nm with a full-width-half-maximum bandwidth of 26 nm. From a single pulse of 600-μJ energy, three pulses each having 4 μJ of energy were independently pulse-shaped and delivered in an unfocused beam with 3 mm diameter.

Figures 2(a) and 2(b) show a typical 2D-FTOS measurement of $P_a(\tau_1,\tau_2)$+$P_b(\tau_1,\tau_2)$ and its Fourier spectrum $S(\omega_1,\omega_2)$, respectively. As described in the Appendix, the first and second pulses excite the ground state atom to $|a\rangle$ first and then to $|b\rangle$, i.e., $|g\rangle \rightarrow |a\rangle \rightarrow |b\rangle$. This transition coherently mixed with the third pulse excitation $|g\rangle \rightarrow |b\rangle$. The quantum interference of these two transition paths is measured in the FT spectra as

$$S(\omega_{ag}-\omega_0,\omega_{bg}-\omega_0) = c_{ag}^{(1)*}(\alpha) c_{ba}^{(2)*}(\beta) c_{bg}^{(1)}(\gamma), \quad (21)$$

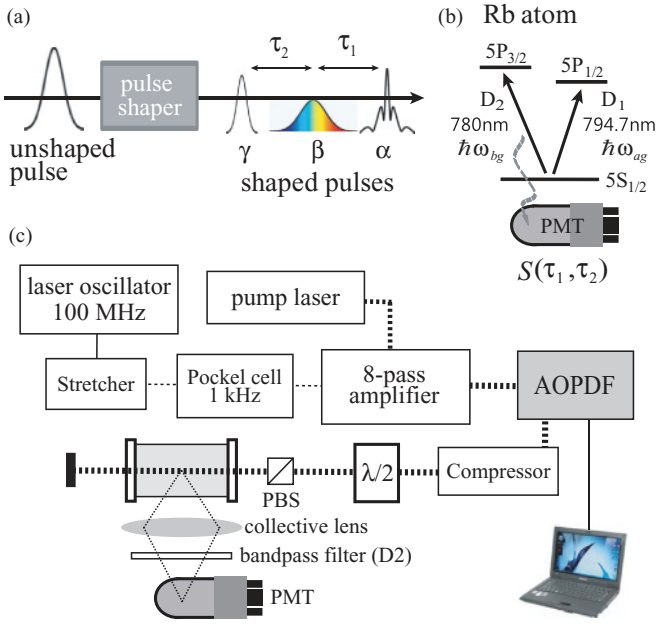

FIG. 1. (Color online) (a) Schematic diagram of three-pulse coherent control scenario. The first pulse has a spectral hole around the D_2 transition, the second pulse is shaped to control the transition probability of the interexcited state transition, and the third pulse is unshaped. (b) The three-pulse sequence was applied to a gaseous Rb atom and the fluorescence at 780 nm was detected with PMT. (c) Experimental setup.

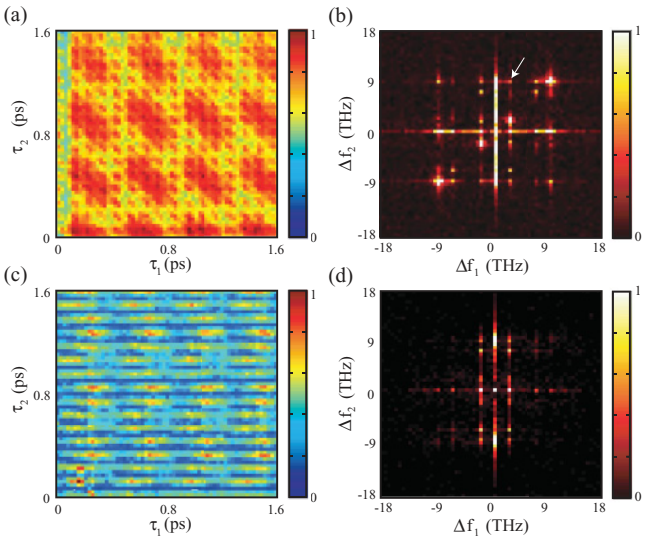

FIG. 2. (Color online) (a) Experimental fluorescence data of 2D-FTOS measurement as a function of two delays, τ_1 and τ_2. (b) 2D Fourier-transformed spectrum $S(\omega_1, \omega_2)$ from the time domain data (a). (c) Fluorescence signal decayed from $|b\rangle$ for the three pulses described in the text and (d) 2D Fourier spectrum of (c).

where $c_{ag}^{(1)}(\alpha)$ and $c_{bg}^{(1)}(\gamma)$ are the one-photon transitions due to the first and third pulses, respectively. They correspond to $\alpha_{ag}^{(1)}$ and $\gamma_{bg}^{(1)}$, respectively, in Eq. (A4). The asterisk denotes the complex conjugate. The off-diagonal peak, marked by the white arrow in Fig. 2(b), represents the controlled transition $c_{ba}^{(2)}(a_2,a_3)$, aside from the constant one-photon transitions. Therefore, the controlled transition from $|a\rangle$ to $|b\rangle$ is well separated from others in the 2D FT spectra.

In the experiment, the first pulse α was shaped to have a spectral hole around the D_2 transition at 780.0 nm. By doing so, the $|g\rangle \rightarrow |b\rangle$ transition is not initiated, which reduces the number of unused spectral peaks in $S(\omega_1,\omega_2)$. The second pulse, the control pulse, was programmed in the spectral domain. The third pulse was not shaped. After the three pulses were applied, the fluorescence spectrally filtered at 780 nm (3-nm bandwidth) was recorded using a photomultiplier tube. Figures 2(c) and 2(d) show correspondingly measured $P_b(\tau_1,\tau_2)$ [without $P_a(\tau_1,\tau_2)$] and its Fourier spectrum for comparison with Figs. 2(a) and 2(b), respectively. Since the primary slow oscillation component decayed from $|a\rangle$ is eliminated by the interference filter, Fig. 2(c) [$P_b(\tau_1,\tau_2)$] should be filled with a speckled pattern. However, due to the spectral hole around the D_2 transition of the first pulse, the coherence between $|g\rangle$ and $|b\rangle$ is annihilated during the delay τ_1 and the slow oscillation dominates the signal along the τ_1 axis. Therefore the higher frequency components of $S(\omega_1,\omega_2)$ in Fig. 2(d) are almost wiped out and the $(\omega_{ag}-\omega_0, \omega_{bg}-\omega_0)$ peak is emphasized. In this way, unwanted higher order transitions affecting $(\omega_{ag}-\omega_0, \omega_{bg}-\omega_0)$ peak and background noises are greatly suppressed.

IV. RESULTS AND DISCUSSION

The proposed two-photon "CT-like behavior" experiments in a V-shape system are shown in Fig. 3. The surface plot in Fig. 3(a) shows results of a numerical calculation of the $5P_{1/2}$–$5P_{3/2}$ transition probability in Eq. (20). The boxed region in Fig. 3(a) was tested using the spectral phase function $\phi(\omega)$ in Eq. (5). The control pulse was programmed with two kinds of chirp coefficients that were uniformly sampled from $a_2 = [-3, 3]\times10^3$ fs^2 and $a_3 = [-5, 7]\times10^4$ fs^3, and the result is shown in Fig. 3(b). The amplitudes extracted from the $(\omega_{ag}-\omega_0, \omega_{bg}-\omega_0)$ peaks in the 2D FT spectra are plotted in Figs. 3(c)–3(e) for $a_3 = -5\times10^4$, -1×10^4, and 3×10^4 fs^3, respectively, together with the theoretical curves calculated from Eq. (20). For a given quadratic chirp, the transition probability shows an oscillatory nature as a function of the linear chirp coefficient, a typical feature of CTs.

Figure 4 illustrates the retrieval of $5P_{1/2}$–$5P_{3/2}$ transition probability amplitude from the coherently controlled 2D spectral peak. The left panel of Fig. 4 (sublabeled with -I) shows $|S(\omega_{ag}-\omega_0,\omega_{bg}-\omega_0)|$, the absolute of the extracted 2D-FTOS peaks. The experimental results (circles) and the calculations (lines) are shown as a function of linear chirp for various quadratic chirps of (a) -5×10^4 fs^3, (b) -3×10^4 fs^3, (c) -1×10^4 fs^3, (d) 1×10^4 fs^3, (e) 3×10^4 fs^3, (f) 5×10^4 fs^3, and (g) 7×10^4 fs^3. The numerical calculations are normalized with the transition probability amplitude at $a_2 = 6\times10^3$ fs^2, $a_3 = 0$, and the experiments accordingly. The experimental results are in good agreement with the numerical calculation.

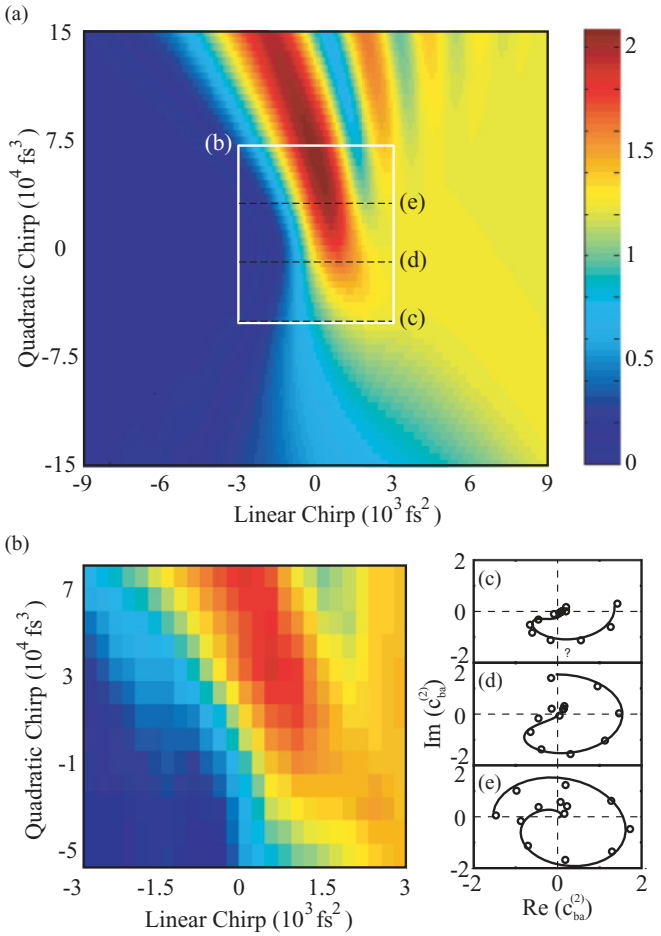

FIG. 3. (Color online) (a) Numerical calculations of the $5P_{1/2}$–$5P_{3/2}$ transition probability amplitude $|c_{ba}^{(2)}|$ as a function of the linear and quadratic chirp. (b) Extracted amplitudes of $(\omega_{ag}-\omega_0, \omega_{bg}-\omega_0)$ peak of the experimentally measured 2D FT spectra (the data were interpolated twice from 13 × 7 measurements.) (c)–(e) Two-photon transition amplitudes $c_{ba}^{(2)}$ in the complex plane as a function of chirp, (c) for quadratic chirp -5×10^4 fs^3, (d) for -1×10^4 fs^3, and (e) for 3×10^4 fs^3.

Finally, the phase information of the $5P_{1/2}$–$5P_{3/2}$ transition probability amplitude is obtained directly from the phase of $(\omega_{ag}-\omega_0, \omega_{bg}-\omega_0)$ peaks in 2D-FTOS spectra. The central panel of Fig. 4 (sublabeled with -II) represents the phase and amplitude of extracted $c_{ba}^{(2)}$. The values start from the origin at a negative linear chirp and spread out by rotating counterclockwise as the linear chirp becomes positive. The well-known Cornu spirals of CTs [20] are reconstructed by compensating the phase difference, $\phi_c = \exp[-i(\overline{\omega}-\omega_0)\omega_{ba}a_2]$, between Eqs. (3) and (20). We note that another phase, $-\frac{1}{2}\tan^{-1} 2\widetilde{a}_2/\widetilde{\tau}_o^2$ in Eq. (20), is already included in $\mathcal{E}_o$ of Eq. (3). The results are summarized in the right panel of Fig. 4 (sublabeled with -III). The phase-compensated transition probability amplitudes, $e^{i\phi_c}c_{ba}^{(2)}$, perfectly reconstruct a Cornu spiral which starts from the origin and approaches to an asymptotic point. It is noted that the asymptotic points have the same radius from the origin for all quadratic chirps, which is equivalent to the fact that the transition probability amplitude of the two-level problem is dependent only on the resonant spectral amplitude $\widetilde{E}(\omega_{21})$ in Eq. (15).

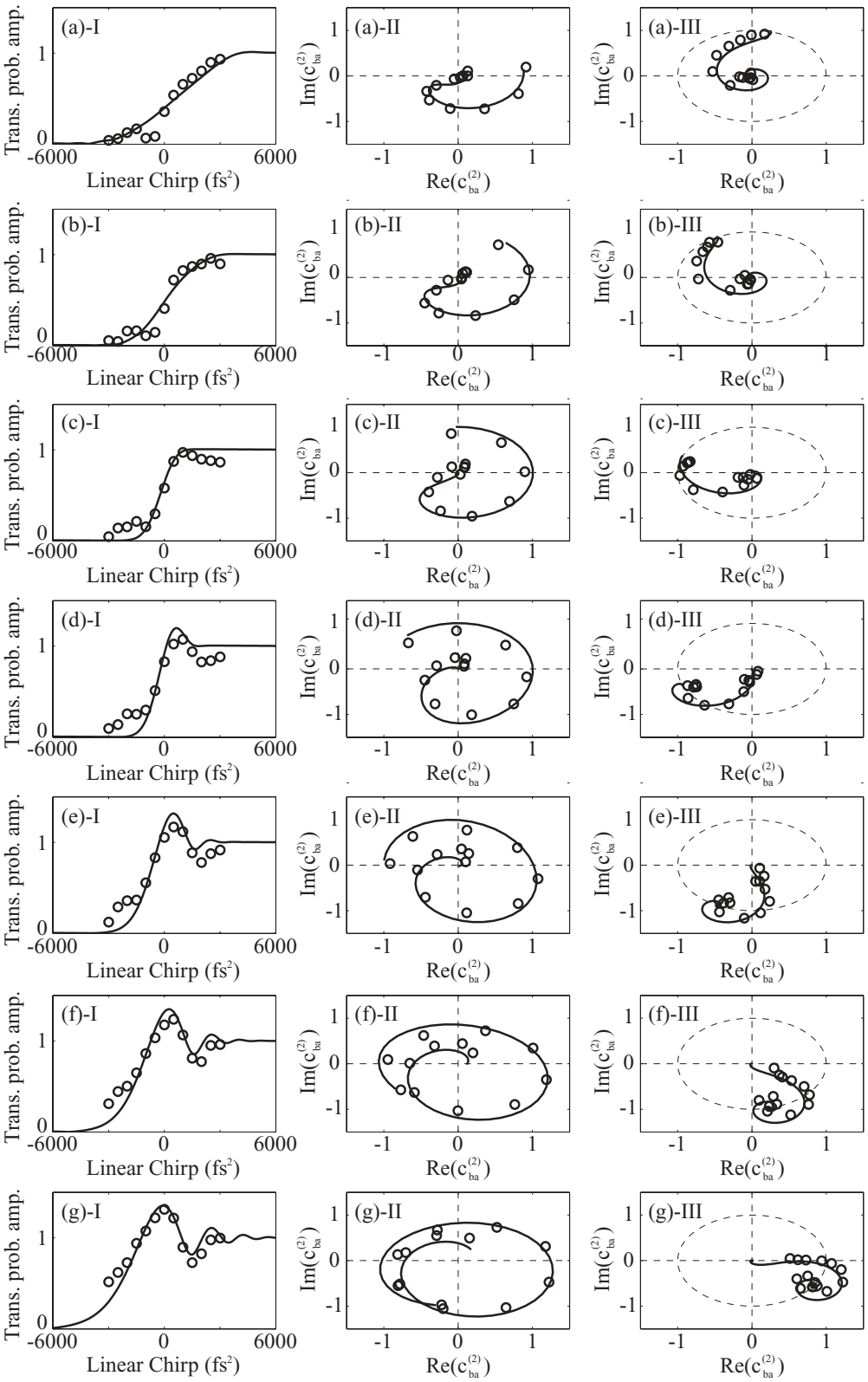

FIG. 4. (a) Extracted transition probabilities from the experimental 2D spectra at ($\omega_{ag} - \omega_0$, $\omega_{bg} - \omega_0$) peaks (circles) together with the numerical calculations of $5P_{1/2}$–$5P_{3/2}$ transition (lines) as a function of linear chirp for quadratic chirp of the second pulse, (a) -5×10^4 fs^3, (b) -3×10^4 fs^3, (c) -1×10^4 fs^3, (d) 1×10^4 fs^3, (e) 3×10^4 fs^3, (f) 5×10^4 fs^3, and (g) 7×10^4 fs^3. The left panel, sublabeled with -I, shows the absolute value of $c_{ba}^{(2)}$, and the central panel (II) is the complex plane representation of $c_{ba}^{(2)}$. The reconstructed Cornu spirals are shown in the right panel (III) following the process explained in the text.

V. CONCLUSIONS

In summary, we have shown that two-photon coherent control in a V-shape three-level system behaves formally like a coherent transient signal in a two-level system, where the roles of time and linear chirp in the latter are duplicated by linear and quadratic chirp rates in the former. For the measurement a three-pulse coherent control scheme is devised, and the phase and amplitude of the controlled transition probability are retrieved from a 2D FT spectral peak.

ACKNOWLEDGMENTS

This research was supported by Basic Science Research and Mid-Career Researcher Programs through the National Research Foundation of Korea (NRF), funded by the Ministry of Education, Science and Technology (No. 2009-0090843, No. 2010-0013899). We thank C. H. Nam for the acousto-optic modulator and also for helpful discussions.

APPENIDX : THREE-PULSE COHERENT CONTROL SCHEME

Measurement of the phase and amplitude of interexcited state transitions can be achieved by using a three-pulse coherent control scheme for a 2D FT spectroscopy.

As our starting point, the quantum system is in the ground state, i.e., $|\psi(t=0-)\rangle = |g\rangle$. By assuming the interaction in the weak field regime [i.e., $V_{ij}(t) \ll \hbar$ for all t], we neglect the higher order terms of $V(t)$ and consider the lowest order terms of each transition. Then the evolution operator for the first pulse is written in terms of three states $\{|g\rangle,|a\rangle,|b\rangle\}$ as

$$U_I(\alpha) = \begin{pmatrix} 1 & \alpha_{ga}^{(1)} & \alpha_{gb}^{(1)} \\ \alpha_{ag}^{(1)} & 1 & \alpha_{ab}^{(2)} \\ \alpha_{bg}^{(1)} & \alpha_{ba}^{(2)} & 1 \end{pmatrix}, \tag{A1}$$

where $\alpha^{(1,2)}$ denote the transition probability amplitudes, respectively defined in Eqs. (11) and (12), for the first pulse. (Likewise, $\beta^{(1,2)}$ and $\gamma^{(1,2)}$ denote the ones for the second and third pulses, in the following.) We note that $\alpha_{ga}^{(1)} = \alpha_{ag}^{(1)*}$ but $\alpha_{ba}^{(2)} \neq \alpha_{ab}^{(2)*}$. Then the wave function after the first interaction is given by $|\psi(0+)\rangle = |g\rangle + \alpha_{ag}^{(1)}|a\rangle + \alpha_{bg}^{(1)}|b\rangle$. For the second pulse, the time delay τ_1 causes an overall phase shift of $\exp[i(\omega_{ng}-\omega_0)\tau_1]$ to the $V_{ij}(t)\exp(i\omega_{ij})$ term in Eqs. (11) and (12), relative to the ones for $\alpha^{(1,2)}$. Therefore, the first- and second-order transition probability amplitudes for the second pulse, including the phase shift from the time delay, are obtained, $\beta_{fi}^{(1)}\exp[i(\omega_{fi}-\omega_0)\tau_1]$ and $\beta_{fi}^{(2)}\exp[i(\omega_{fg}-\omega_0)\tau_1 - i(\omega_{ig}-\omega_0)\tau_1]$, respectively, where the rotating wave approximation is used for $\beta_{ba}^{(2)}$. Accordingly, the evolution operator for the second pulse, including the time delay effect, is given by

$$U_I(\beta) = \begin{pmatrix} 1 & \beta_{ag}^{(1)*}e^{-i\Delta\omega_{ag}\tau_1} & \beta_{bg}^{(1)*}e^{-i\Delta\omega_{bg}\tau_1} \\ \beta_{ag}^{(1)}e^{i\Delta\omega_{ag}\tau_1} & 1 & \beta_{ab}^{(2)}e^{i(\Delta\omega_{ag}-\Delta\omega_{bg})\tau_1} \\ \beta_{bg}^{(1)}e^{i\Delta\omega_{bg}\tau_1} & \beta_{ba}^{(2)}e^{-i(\Delta\omega_{ag}-\Delta\omega_{bg})\tau_1} & 1 \end{pmatrix}, \tag{A2}$$

where $\Delta\omega_{ij} = \omega_{ij} - \omega_0$. After the second pulse the wave function becomes $|\psi(\tau_1)\rangle = U_I(\beta)|\psi(0+)\rangle$. Likewise, the evolution operator for the third pulse, including the effect of the time delay τ_2 relative to the second pulse, is given by

$$U_I(\gamma) = \begin{pmatrix} 1 & \gamma_{ag}^{(1)*}e^{-i\Delta\omega_{ag}(\tau_1+\tau_2)} & \gamma_{bg}^{(1)*}e^{-i\Delta\omega_{bg}(\tau_1+\tau_2)} \\ \gamma_{ag}^{(1)}e^{i\Delta\omega_{ag}(\tau_1+\tau_2)} & 1 & \gamma_{ab}^{(2)}e^{i(\Delta\omega_{ag}-\Delta\omega_{bg})(\tau_1+\tau_2)} \\ \gamma_{bg}^{(1)}e^{i\Delta\omega_{bg}(\tau_1+\tau_2)} & \gamma_{ba}^{(2)}e^{-i(\Delta\omega_{ag}-\Delta\omega_{bg})(\tau_1+\tau_2)} & 1 \end{pmatrix}, \tag{A3}$$

and after the all three pulsed interactions, the final wave function $|\psi(\tau_1+\tau_2)\rangle$ is obtained as the sum of 27 different terms. By measuring the projection to $|b\rangle$ state, the probability $P_b = |\langle b|\psi\rangle|^2$ is given by

$$P_b(\tau_1,\tau_2) = \left|\alpha_{bg}^{(1)}\right|^2 + \left|\beta_{bg}^{(1)}\right|^2 + \left|\gamma_{bg}^{(1)}\right|^2 + \ldots + \alpha_{ag}^{(1)*}\beta_{ba}^{(2)*}\gamma_{bg}^{(1)}e^{i(\Delta\omega_{ag}\tau_1+\Delta\omega_{bg}\tau_2)} + \ldots, \tag{A4}$$

where, for example, the term $\alpha_{ag}^{(1)*}\beta_{ba}^{(2)*}\gamma_{bg}^{(1)}\exp(i\Delta\omega_{ag}\tau_1 + i\Delta\omega_{bg}\tau_2)$ denotes the quantum interference between the two transitions $|g\rangle \to |a\rangle \to |b\rangle$ and $|g\rangle \to |b\rangle$. The coefficient $\alpha_{ag}^{(1)*}\beta_{ba}^{(2)*}\gamma_{bg}^{(1)}$ is retrieved from $|\langle b|\psi\rangle|^2$ as the amplitude and phase of the temporally modulated component with the function $\exp(i\Delta\omega_{ag}\tau_1 + i\Delta\omega_{bg}\tau_2)$. The modulation $\exp(i\Delta\omega_{ag}\tau_1)$ and $\exp(i\Delta\omega_{bg}\tau_2)$ are from the phase evolution that the atoms are respectively in state $|a\rangle$ during τ_1 and in state $|b\rangle$ during τ_2. The 2D FT spectrum is defined as

$$S(\omega_1,\omega_2) = \int\int P_b(\tau_1,\tau_2)e^{-i(\omega_1\tau_1+\omega_2\tau_2)}d\tau_1 d\tau_2, \tag{A5}$$

which has 49 peaks including a zero-frequency peak. The coefficients of the spectral peaks of $S(\omega_1,\omega_2)$ in the first quadrant of the 2D plane are listed in Table I. Aside from the constant $\alpha_{ag}^{(1)*}\gamma_{bg}^{(1)}$, the controlled transition probability amplitude $\beta_{ba}^{(2)*}$ is then retrieved from the peak located at $(\omega_1,$

TABLE I. Peaks in the first quadrant of a 2D FT plane of $|\langle b|\psi\rangle|^2$. For example, the peak at $(\Delta\omega_{ag}, \Delta\omega_{bg})$ represents the quantum interference between $|g\rangle \rightarrow |a\rangle \rightarrow |b\rangle$ and $|g\rangle \rightarrow |b\rangle$ transitions.

$\omega_2 \setminus \omega_1$	$\Delta\omega_{ag}$	$\Delta\omega_{bg} - \Delta\omega_{ag}$	$\Delta\omega_{bg}$
$\Delta\omega_{bg}$	$\alpha_{ag}^{(1)*}\beta_{ba}^{(2)*}\gamma_{bg}^{(1)}$	$\alpha_{ag}^{(1)}\alpha_{bg}^{(1)*}\beta_{ag}^{(1)*}\gamma_{bg}^{(1)}$	$\alpha_{bg}^{(1)*}\gamma_{bg}^{(1)}$
$\Delta\omega_{bg} - \Delta\omega_{ag}$	$\alpha_{ag}^{(1)*}\beta_{ag}^{(1)}\beta_{ba}^{(2)*}\gamma_{ba}^{(2)}$	$\alpha_{ag}^{(1)}\alpha_{bg}^{(1)*}\gamma_{ba}^{(2)}$	$\alpha_{bg}^{(1)*}\beta_{ag}^{(1)}\gamma_{ba}^{(2)}$
$\Delta\omega_{ag}$	$\alpha_{ag}^{(1)*}\gamma_{bg}^{(1)}\gamma_{ba}^{(2)*}$	$\alpha_{ag}^{(1)}\alpha_{bg}^{(1)*}\beta_{ag}^{(1)*}\beta_{ab}^{(2)*}\gamma_{bg}^{(1)}\gamma_{ba}^{(2)*}$	$\alpha_{bg}^{(1)*}\beta_{ab}^{(2)*}\gamma_{bg}^{(1)}\gamma_{ba}^{(2)*}$

$\omega_2) = (\Delta\omega_{ag}, \Delta\omega_{bg})$. As a result, the three-pulse coherent control scheme devised for 2D FT spectroscopy can be used to measure the two-photon interexcited state transition coefficients.

[1] A. M. Weiner, Rev. Sci. Instrum. **71**, 1929 (2000).
[2] H. Rabitz, R. de Vivie-Riedle, M. Motzkus, and K. Kompa, Science **288**, 824 (2000).
[3] M. Shapiro and P. Brumer, *Principles of the Quantum Control of Molecular Processes* (Wiley, New York, 2003).
[4] D. J. Tanner and S. A. Rice, J. Chem. Phys. **83**, 5013 (1985).
[5] T. C. Weinacht, J. Ahn, and P. H. Bucksbaum, Nature **397**, 233 (1999).
[6] R. S. Judson and H. Rabitz, Phys. Rev. Lett. **68**, 1500 (1992).
[7] K. Bergmann, H. Theuer, and B. W. Shore, Rev. Mod. Phys. **70**, 1003 (1998).
[8] P. Nuernberger, G. Vogt, T. Brixner, and G. Gerber, Phys. Chem. Chem. Phys. **9**, 2470 (2007).
[9] C. J. Bardeen, V. V. Yakovlev, J. A. Squier, and K. R. Wilson, J. Am. Chem. Soc. **120**, 13023 (1998).
[10] S. Chelkowski and A. D. Baundrauk, J. Chem. Phys. **99**, 4279 (1993).
[11] B. Amstrup, G. Szabo, R. A. Sauebrey *et al.*, Chem. Phys. **188**, 87 (1994).
[12] U. Gaubatz, P. Rudecki, S. Schiemann, and K. Bergmann, J. Chem. Phys. **92**, 5363 (1990).
[13] J. Karczmarek, J. Wright, P. Corkum, and M. Ivanov, Phys. Rev. Lett. **82**, 3420 (1999).
[14] D. G. Lee, J. H. Kim, K. H. Hong, and C. H. Nam, Phys. Rev. Lett. **87**, 243902 (2001).
[15] N. Dudovich, B. Dayan, S. M. GallagherFaeder, and Y. Silberberg, Phys. Rev. Lett. **86**, 47 (2001).
[16] J. Degert, W. Wohlleben, B. Chatel, M. Motzkus, and B. Girard, Phys. Rev. Lett. **89**, 203003 (2002).
[17] S. Zamith, J. Degert, S. Stock, B. de Beauvoir, V. Blanchet, M. A. Bouchene, and B. Girard, Phys. Rev. Lett. **87**, 033001 (2001).
[18] E. Hecht, *Optics* (Addison Wesley, 2002), 4th ed.
[19] N. Dudovich, D. Oron, and Y. Silberberg, Phys. Rev. Lett. **88**, 123004 (2002).
[20] A. Monmayrant, B. Chatel, and B. Girard, Phys. Rev. Lett. **96**, 103002 (2006).
[21] W. Merkel, H. Mack, W. P. Schleich, E. Lutz, G. G. Paulus, and B. Girard, Phys. Rev. A **76**, 023417 (2007).
[22] R. Netz, T. Feurer, G. Roberts, and R. Sauerbrey, Phys. Rev. A **65**, 043406 (2002).
[23] N. Dudovich, D. Oron, and Y. Silberberg, Phys. Rev. Lett. **88**, 123004 (2002).
[24] L. Chuntonov, L. Rybak, A. Gandman, and Z. Amitay, Phys. Rev. A **77**, 021403 (2008).
[25] S. D. Clow, C. Trallero-Herrero, T. Bergeman, and T. Weinacht, Phys. Rev. Lett. **100**, 233603 (2008).
[26] S. Lee, J. Lim, and J. Ahn, Opt. Express **17**, 7648 (2009).
[27] D. Keusters, H.-S. Tan, and W. S. Warren, J. Phys. Chem. A **103**, 10369 (1999).
[28] D. M. Jonas, Annu. Rev. Phys. Chem. **54**, 425 (2003).
[29] K. W. Stone, K. Gundogdu, D. B. Turner, X. Li, S. T. Cundiff, and K. A. Nelson, Science **324**, 1169 (2009).
[30] F. Verluise, V. Laude, Z. Cheng, Ch. Spielmann, and P. Tournois, Opt. Lett. **25**, 575 (2000).